IMMUNOLOGY

Adjuvant-free nanofiber vaccine induces in situ lung dendritic cell activation and T_H17 responses

Youhui Si[1], Qiaomu Tian[1], Fan Zhao[1], Sean H. Kelly[2], Lucas S. Shores[2], Daniel F. Camacho[3], Anne I. Sperling[3], Michael S. Andrade[1], Joel H. Collier[2]*, Anita S. Chong[1]*

The current paradigm that subunit vaccines require adjuvants to optimally activate innate immunity implies that increased vaccine reactogenicity will invariably be linked to improved immunogenicity. Countering this paradigm, nanoparticulate vaccines have been reported to act as delivery systems for vaccine antigens and induce immunity without the need for exogenous adjuvants or local inflammation; however, the mechanisms underlying the immunogenicity of nanoparticle vaccines are incompletely identified. Here, we show that antigens displayed on self-assembling nanofiber scaffolds and delivered intranasally are presented by $CD103^+$ and $CD11b^+$ lung dendritic cells that up-regulate CD80 and migrate into the draining lymph node (LN). This was accompanied by a nearly exclusive priming and accumulation of antigen-specific T_H17 cells occurring independently in both LN and lung. Thus, self-assembling peptide nanofiber vaccines may represent a novel, needle- and adjuvant-free means of eliciting protective immunity against fungal and bacterial infections at skin and mucosal barrier surfaces.

INTRODUCTION

Intranasal vaccination has received growing interest because it is needle-free and elicits tissue-resident memory T cells that provide more rapid and better protection within targeted tissues. The nasal route of delivery of low–molecular weight drugs has already been approved for clinical use [reviewed in (*1*)], and despite increasing interest in the intranasal delivery of vaccines, their clinical application has been limited to the live attenuated influenza vaccine (FluMist). In contrast, intranasal subunit vaccines have only advanced to preclinical studies in rodents, and none have reached the clinical market due, at least in part, to low intranasal uptake for large molecules and the requirement for proinflammatory adjuvants to improve immunogenicity (*2*). Adjuvants elicit unacceptable inflammation in the lung, and more work is required to define approaches that increase the immunogenicity of intranasal subunit vaccines without also enhancing reactogenicity.

The current paradigm of adjuvants inducing the early activation of innate immunity through inflammation or danger signals implies that increased vaccine reactogenicity will invariably be linked to improved immunogenicity. While there are increasing number of adjuvants recently approved for human use, including aluminum salts, emulsions (MF59, AS03), and Toll-like receptor agonists [CpG, monophosphoryl lipid A (MPL)], adverse reactions continue to plague these adjuvants and are often cited as reasons for reduced vaccine compliance [reviewed in (*3*)]. Common adverse reactogenicities include local swelling and pain, systemic fever, and malaise, while rare reactions include the aberrant triggering immune activation and autoimmune diseases, narcolepsy, and marcrophagic myofasciitis. Thus, an alternative hypothesis of a potent noninflammatory vaccine that avoids reactogenicity warrants further investigation as a means to safer effective vaccines. Solis *et al.* (*4*) recently reported that myeloid cells in the lung are able to sense cyclical hydrostatic pressure and initiate an inflammatory response, underscoring a novel role for mechanosensation in regulating innate immunity.

Growing interest in nanoparticulate vaccines has been fueled by reports that they can act both as delivery systems for vaccine antigens and as immunomodulators (*5*). We and others have previously reported that the Q11 peptide scaffold system, in which short synthetic peptides self-assemble into fibers with lengths of hundreds of nanometers or more, and widths of approximately 10 to 20 nm, can raise T cell or B cell epitope-specific immune responses (*6*–*8*, *9*). These immune responses are raised without supplemental adjuvants, although immune responses can be boosted when the Q11 nanofibers are coimmunized with adjuvants (*8*). Furthermore, because Q11 nanofibers are able to raise adaptive immune responses with minimal local inflammation, the character of the elicited immune response can be adjusted based on controllable parameters such as the density of T or B cell epitopes and the ratio between T and B cell epitopes (*7*). While our early studies have focused on the subcutaneous delivery of Q11 nanofiber vaccines and the resulting $CD4^+$ T cell or antibody responses, we recently reported that self-assembled peptide nanofibers bearing a class I–restricted peptide epitope, derived from influenza polymerase (PA) and delivered either subcutaneously or intranasally, were able to elicit PA-specific $CD8^+$ T effector cell responses (*9*). Notably, both circulating and lung-resident memory $CD8^+$ T cells were elicited, and those memory cells were rapidly reactivated upon subsequent influenza infection.

In this study, we test the hypothesis that intranasal Q11 vaccines are taken up by dendritic cells (DCs), which then process and present antigen productively to T cells in the draining lymph node (LN). We previously reported that the intraperitoneal delivery of these nanofibers results in their uptake by peritoneal DCs and macrophages and presentation of antigen by peritoneal DCs (*6*). However, we could not detect DCs presenting Q11 vaccine antigens in the draining LN, where adaptive T cell and antibody responses are initiated. In the current study, we successfully identify lung $CD103^+$cDC1 and $CD11b^+$cDC2 as the major antigen-presenting cells (APCs) following the intranasally delivery of Q11 nanofibers carrying the pEα peptide antigen (EαQ11). The pEα epitope is derived from the major histocompatibility complex class II (MHCII) I-E^dα chain

[1]Department of Surgery, The University of Chicago, Chicago, IL 60637, USA. [2]Biomedical Engineering Department, Duke University, Durham, NC 27708, USA. [3]Department of Medicine, The University of Chicago, Chicago, IL 60637, USA.
*Corresponding author. Email: achong@uchicago.edu (A.S.C.); joel.collier@duke.edu (J.H.C.)

(α_{52-68} peptide), and pEα:I-A^b complexes on APC can be detected with the pEα:I-A^b–specific Y-Ae monoclonal antibody (mAb) (*10*). Using this antigen system, we show that pEα:I-A^b–positive lung DCs up-regulate CD80 and migrate into the draining mediastinal LN (MLN), where they are the major source of pEα:I-A^b–positive DCs. Furthermore, we show that intranasal delivery of EαQ11 nanofibers promotes the differentiation of TEa almost exclusively into T helper 17 (T_H17) cells. Last, we confirm that EαQ11 vaccines induce the accumulation of TEa T cells, which express the T cell receptor (TCR) specific for pEα:I-A^b (*11*), and show that, unexpectedly, TEa priming occurred independently in both the lung and draining LN.

RESULTS

DCs are the main APCs in the lung and draining LN after intranasal immunization with Q11-Eα nanofibers

The lung has evolved to ward off infections while simultaneously restraining inflammation-mediated injury, and harbors three different cell types potentially capable of antigen uptake and presentation, namely, DCs, macrophages, and B cells. Lung-resident macrophages and DCs are located in close proximity to the epithelial surface of the respiratory system, where they are able to sample inhaled material entering the lung [reviewed in (*12*)]. Tissue-resident B cell clones have recently been shown to partition into two broad networks in humans: One spans the blood, bone marrow, spleen, and lung, while the other is restricted to the gastrointestinal tract. However, the precise location of the B cells within each of these organs, including the lung, remains unclear.

We previously reported that DCs are essential for the ability of intraperitoneally administered Q11-OVA (ovalbumin) nanofibers (*6*, *13*) to stimulate antibody and $CD4^+$ T cell responses and for intranasally administered Q11-based vaccines to elicit effector and tissue-resident memory $CD8^+$ T cells (*9*). Immunogenic Q11 nanofibers can drain directly to the LN where they are taken up by LN-resident APCs, or they can be taken up by lung APCs that then migrate to the draining LN. To identify the APCs that are able to capture and present antigen in the lung and draining LN, we generated Q11 nanofibers carrying the pEα peptide antigen (EαQ11). On transmission electron microscopy (TEM) grids, unsheared EαQ11 nanofibers formed an entangled mat of nanofibers (~350 nm long) (Fig. 1, A and B). Following intranasal immunization with EαQ11, we harvested DCs, macrophages, and B cells from the lung 2 days after vaccination (Fig. 1C and fig. S1). pEα:I-A^b complexes were detected on $MHCII^{hi}$,$CD11c^+$ DCs, while minimal numbers of Siglec F^+CD11c^+ macrophages or $MHCII^{hi}$ $CD19^+$ B cells expressed pEα:I-A^b (Fig. 1, D and E). Likewise, DCs were the predominant APC presenting pEα:I-A^b complexes in the MLN (Fig. 1F). No pEα:I-A^b–positive DCs in the lung or MLN were detected in mice receiving Q11 nanofibers without pEα. Last, to test the necessity for intact nanofibers, EαQ11 nanofibers were sheared through a polycarbonate membrane containing 0.2-μm laser track-etched pores to yield nanofibers that were significantly shorter (~100 nm; Fig. 1, A and B). Reduced antigen presentation by lung and LN DCs was observed following immunization with sheared EαQ11, suggesting that the length of Q11 nanofibers following intranasal delivery determines optimal presentation of attached antigen (Fig. 1, D to F).

Lung DCs can be categorized into conventional $CD103^+$cDC1, $CD11b^+$cDC2, and plasmacytoid DCs, each subset representing an independent developmental lineage and having distinct but overlapping functions (*12*, *14*). We focused on $CD103^+$cDC1 and $CD11b^+$ cDC2 subsets in the lung and MLN and observed that both subsets presented pEα:I-A^b (Fig. 1, G and H, and fig. S1). We did not observe significant increases in the numbers of pEα:I-A^b DCs in the cervical LN on day 4 after intranasal immunization (fig. S2). These observations confirm previous reports (*15*) that the mediastinal is the main LN draining the lung. These observations are consistent with the hypothesis that lung DCs take up EαQ11 nanofibers, process and present the pEα antigen, and then migrate to the draining LN to present pEα:I-A^b to $CD4^+$ T cells.

Kinetics of antigen presentation in the lung and draining LNs

To test the hypothesis that lung DCs are the primary source of pEα-presenting cells in the draining LN, we performed detailed kinetics on the appearance of pEα:I-A^b–positive DCs in the lung and MLN following intranasal vaccination with EαQ11 nanofibers (Fig. 2A). A trend toward a modest increase in total $CD11b^+$ DCs in the lung was observed on days 1 to 2 after vaccination (Fig. 2B), and a greater, statistically significant, increase in the numbers of pEα:I-A^b–positive $CD11b^+$ and $CD103^+$ DCs in the lung were observed on days 1 to 3 after vaccination (Fig. 2C). A modest increase in the numbers of total $CD11b^+$ and $CD103^+$ DCs was observed in the MLN on days 3 and 4 after vaccination (Fig. 2D), with a greater fold increase in the numbers of pEα:I-A^b–positive DCs that peaked on days 3 to 5 after vaccination (Fig. 2E). These observations are consistent with activation and migration of antigen-presenting DCs into the draining LNs.

We next examined the expression of CD80 as a marker for DC activation of all DCs from the lung and draining LN (Fig. 2F). Total lung DCs from EαQ11-immunized mice expressed significantly elevated levels of CD80 compared to nonimmunized mice, whereas no such increase was observed for the DCs from draining LN. When the DCs were separated into pEα:I-A^b–negative or pEα:I-A^b–positive subsets, DCs that were pEα:I-A^b–positive more strongly up-regulated CD80 compared to pEα:I-A^b–negative DCs (Fig. 2, G and H). A modestly elevated CD80 by pEα:I-A^b–negative lung DCs suggests either bystander activation or that those DCs had taken up EαQ11 but had not processed and presented pEα:I-A^b at the time of analysis. Furthermore, pEα:I-A^b–positive DCs in the lung and MLN expressed significantly elevated CD80, from days 1 to 6 after vaccination, compared to pEα:I-A^b–negative DCs (Fig. 2I). These observations suggest that vaccination with EαQ11 nanofibers resulted in the preferential activation of pEα:I-A^b–positive DCs in the lung, resulting in their increased expression of CD80 and migration to draining LNs, where they also exhibited increased CD80.

Lung pEα:I-A^b–positive DCs migrate into the draining LNs

To more directly demonstrate the migration of lung DCs into the MLN, we first stained DCs already in the lung with PKH26 at 4 hours before intranasal EαQ11 vaccination. The fluorescent dye PKH26 binds to cell membranes without inhibition of cell proliferation or toxicity and has been used to track the migration of cells in vivo (*16*). $PKH26^+$ DCs in the lung and draining LN that expressed pEα:I-A^b complexes were quantified on day 2 after vaccination (Fig. 3, A and B, and fig. S3). Approximately 40% of all $MHCII^{hi}$ cells from the lung, including the $CD11b^+$ and $CD103^+$ DCs, stained positive for PKH26, reflecting incomplete labeling of the resident $MHCII^{hi}$ cells in the lung. Of the $PKH26^+$ cDC1 and cDC2 DCs in the lung, approximately 27 and 55% were positive for pEα:I-A^b following EαQ11 vaccination; in

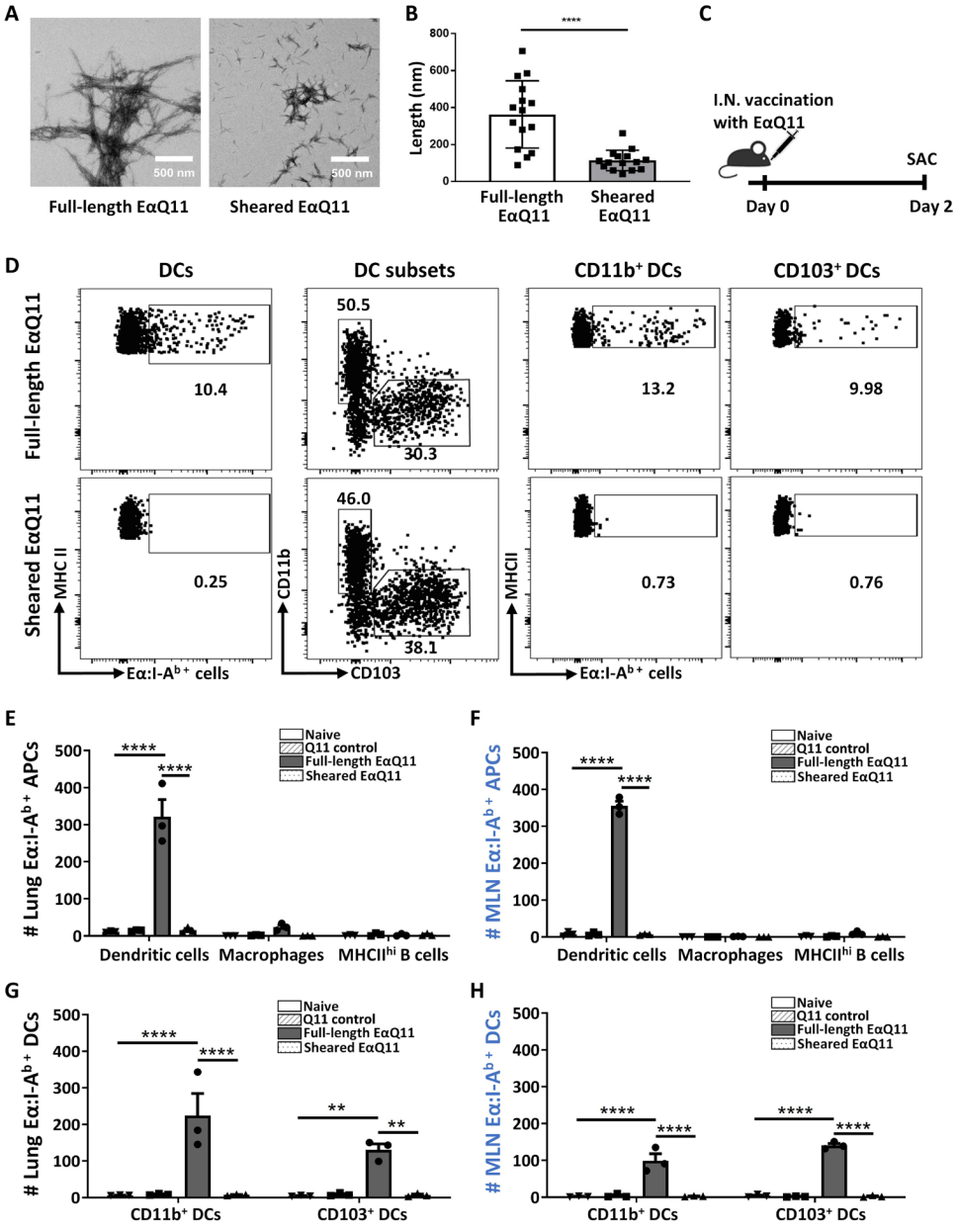

Fig. 1. Integrity of EαQ11nanofibers is required for DC presentation of pEα:I-A^b. (**A**) Negative-stained TEM images of EαQ11 before (left) and after (right) shearing to reduce nanofiber length. (**B**) Lengths were quantified by tracing nanofibers using ImageJ software ($n = 15$ per group). ****$P < 0.0001$ by unpaired, two-tailed t test. (**C**) Scheme of experiment. C57BL/6 mice were intranasally (I.N.) immunized with EαQ11. Lung and MLN were collected on day 2 after vaccination. (**D**) Representative flow cytometry plots displaying pEα:I-A^b–positive CD11b$^+$ or CD103$^+$ DCs in the lung. DCs were identified as CD45$^+$CD49b$^-$TER119$^-$CD19$^-$CD3$^-$SiglecF$^-$Ly6G$^-$CD11c$^+$MHCII^{hi} cells. pEα:I-A^b–positive DCs were detected using the YAe antibody, which recognizes the pEα:I-A^b complex. The number of pEα:I-A^b–positive APCs in lung (**E**; black labels) and MLN (**F**; blue labels). The number of pEα:I-A^b–positive CD11b$^+$/CD103$^+$ DCs in lung (**G**) and MLN (**H**). Each dot represents two pooled mice. Data shown are means ± SEM from three independent experiments. ****$P < 0.0001$ and **$P < 0.01$ by two-way ANOVA (E to H).

the absence of immunization, there were no detectable PKH26$^+$ pEα:I-A^b–expressing DCs in the lung. Approximately 21.4% of all MHCII^{hi} cells in the MLN were PKH26$^+$ in vaccinated mice, whereas significantly fewer (1.2%) were observed in naïve mice, suggesting that intranasal vaccination prompted the overall migration of lung MHCII^{hi} cells into the LN (Fig. 3B).

In a kinetics study, we observed that the total numbers of PKH26$^+$ and PKH26$^+$pEα:I-A^b–positive DCs in the lung increased on days 1 to 2 after EαQ11 vaccination (Fig. 3, C and D). We speculate that this increase in the numbers of PKH26-labeled cells after vaccination is due to the recruitment of circulating DC into the lung that then took up residual PKH26 remaining in the lung (*17*). The total numbers of PKH26$^+$ and PKH26$^+$pEα:I-A^b–expressing CD11b$^+$ and CD103$^+$ DCs in the draining LN significantly increased on days 3 to 5 after vaccination (Fig. 3, E and F). The delayed kinetics of PKH26$^+$pEα:I-A^b–positive DCs appearing in the LN compared to the lung is consistent

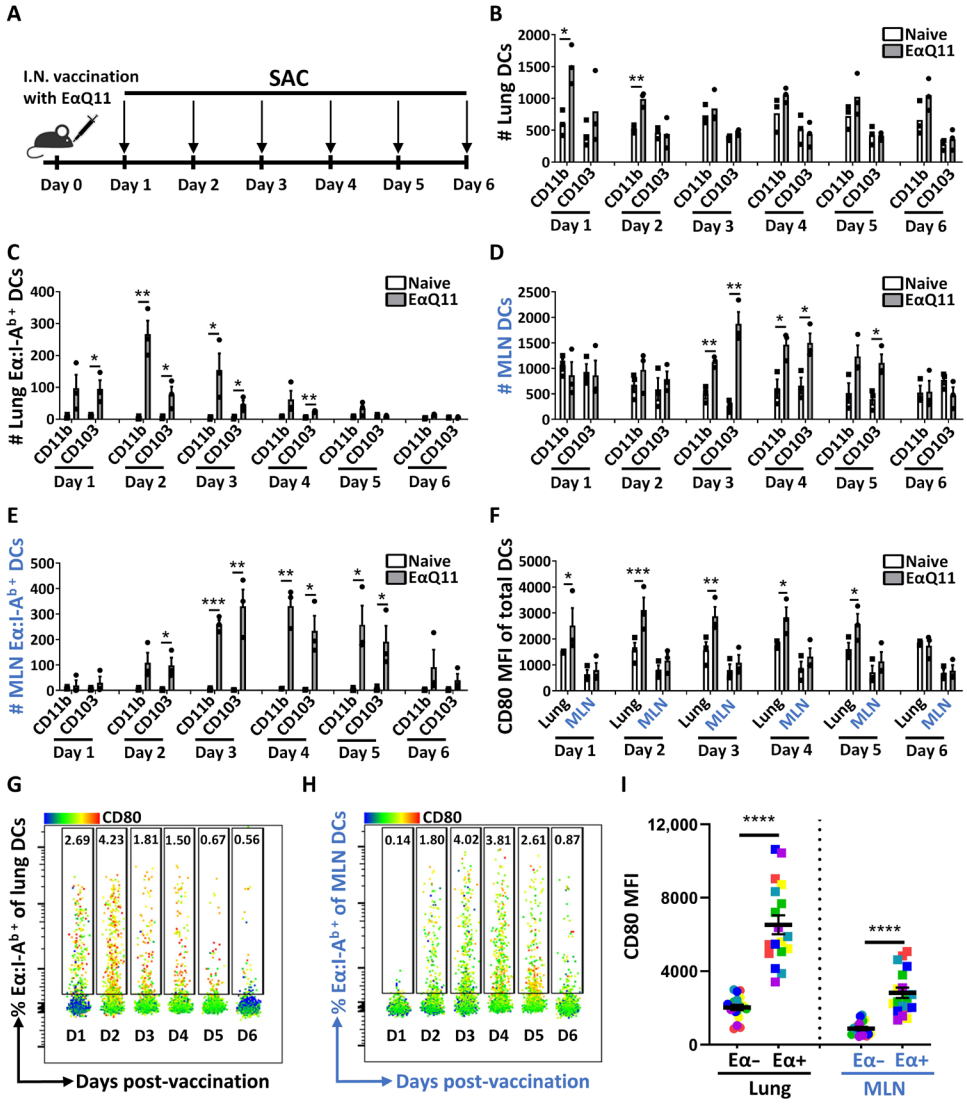

Fig. 2. Kinetic analysis of antigen presentation by DCs in lung and MLNs after EαQ11 intranasal immunization. (**A**) Scheme of experiment. C57BL/6 mice were intranasally immunized with EαQ11. Lung and MLN were collected at the indicated day after immunization. The number of total (**B**) and pEα:I-A^b–positive CD11b$^+$/CD103$^+$ (**C**) DCs in lung. The number of total (**D**) and pEα:I-A^b–positive CD11b$^+$ or CD103$^+$ (**E**) DCs in MLN. (**F**) MFI of CD80 expression on all DCs in naive or immunized mice. Flow plots displaying the relative expression of CD80 as a heatmap on Eα:I-A^{b+} or Eα:I-A^{b-} DCs at the indicated time points in the lung (**G**) or MLN (**H**). Numbers at the top of the flow plots are the percentages of Eα:I-A^{b+} of total DCs. (**I**) MFI of CD80 on Eα:I-A^{b+} or Eα:I-A^{b-} DCs in the lung (black labels) or MLN (blue labels). Each dot is color-coded to indicate different days after vaccination: day 1 (~16 to 18 hours after immunization), red; day 2, yellow; day 3, green; day 4, cyan; day 5, blue; day 6, purple. Each dot represents the results from two pooled mice. Data shown are means ± SEM from three independent experiments. ****$P < 0.0001$, ***$P < 0.001$, **$P < 0.01$, and *$P < 0.05$ by unpaired, two-tailed *t* test (B to F and I).

with a subset of lung DCs presenting the vaccine antigen migrating into the draining LN.

To test whether the majority of the pEα:I-A^b–positive DCs in the draining LN were derived from lung DCs rather than LN-resident DCs, we treated mice with pertussis toxin (PTX) 1 hour before vaccination (Fig. 4A). The key chemokines directing DC migration from sites of infection to LNs include CCL19 and CCL21 binding to CCR7, and conventional DCs (cDCs) lacking CCR7 fail to migrate to LN (*18*). PTX is a protein-based exotoxin produced by Bordetella pertussis that inhibits Gαi protein receptor signal transduction and cell migration in response to chemokines (*19*). Treatment with PTX did not alter the number of all DCs, or Eα-presenting CD11b$^+$ DCs in the lung, but reduced Eα-presenting CD103$^+$ DCs numbers, suggesting a chemokine-driven recruitment of this DC subset into the lung following intranasal vaccination (Fig. 4, B to D). In contrast, mice treated with PTX had significantly reduced numbers of all and Eα-presenting CD11b$^+$ and CD103$^+$ DCs in the MLN, consistent with the conclusion that the majority of the Eα-presenting cells in the draining LN were migrants from the lung (Fig. 4, E and F).

Intranasal immunization with EαQ11 nanofibers elicits a predominantly T_H17 response

We next investigated the effector subsets elicited in adoptively transferred (AdT) TEa cells, which are specific for pEα:I-A^b, following

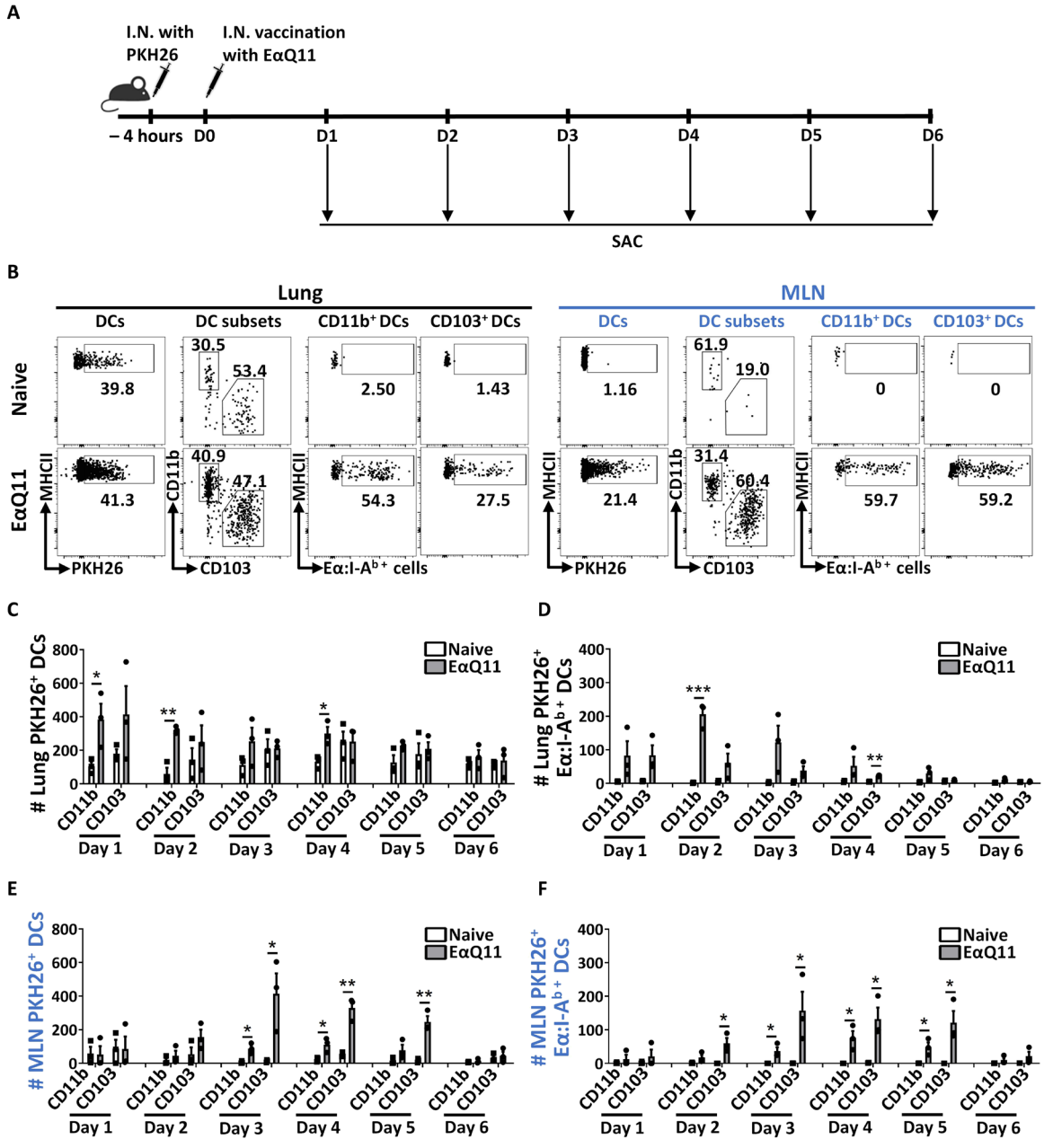

Fig. 3. Lung DCs migrate to MLN after EαQ11 intranasal immunization. (**A**) Scheme of experiment. Lung DCs were labeled with PKH26 in vivo 4 hours before EαQ11 intranasal immunization. PKH26$^+$ DCs were detected in MLN at the indicated day after immunization and considered as lung-derived DCs. (**B**) Representative flow cytometry plots displaying PKH26$^+$ Eα presenting CD11b$^+$/CD103$^+$ DCs in lung (left; black labels) and MLN (right; blue labels). The number of total PKH26$^+$ (**C**) and PKH26$^+$ pEα:I-A^b–positive CD11b$^+$/CD103$^+$ (**D**) DCs in lung. The number of total PKH26$^+$ (**E**) and PKH26$^+$ pEα:I-A^b–positive CD11b$^+$/CD103$^+$ (**F**) DCs in MLN. Note that day 1 mice were examined at ~16 to 18 hours after immunization. Each dot represents two pooled mice. Data shown are means ± SEM from three independent experiments. ***$P < 0.001$, **$P < 0.01$, and *$P < 0.05$ by unpaired, two-tailed t test (C to F).

EαQ11 intranasal vaccination. TEa cells (500,000 per mouse) were AdT on day −1, harvested on day 5 after vaccination, and stained for the transcription factors T-bet, Gata3, RORγt, and FoxP3, which characterize T_H1, T_H2, T_H17, and regulatory T cells (T_{regs}), respectively, while T follicular helper (T_{FH}) cells were identified by their expression of Bcl6 and PD-1 (Fig. 5A and fig. S4). In the lung, approximately 35 and 5% of TEa cells in the lung and MLN, respectively, were RORγt$^+$, compared to <1% in nonvaccinated controls (Fig. 5, B and D). The total numbers of RORγt$^+$ TEa cells in the lung and LN were also significantly higher than those expressing Tbet, Gata3, FoxP3, Bcl6, or PD-1 (Fig. 5, C and E). Similarly, EαQ11 nanofibers elicited a predominant RORγt response by endogenous CD4$^+$ T cells (Fig. 5, F to I), although a statistically significant increase in endogenous T_{regs} was observed in the MLN following immunization.

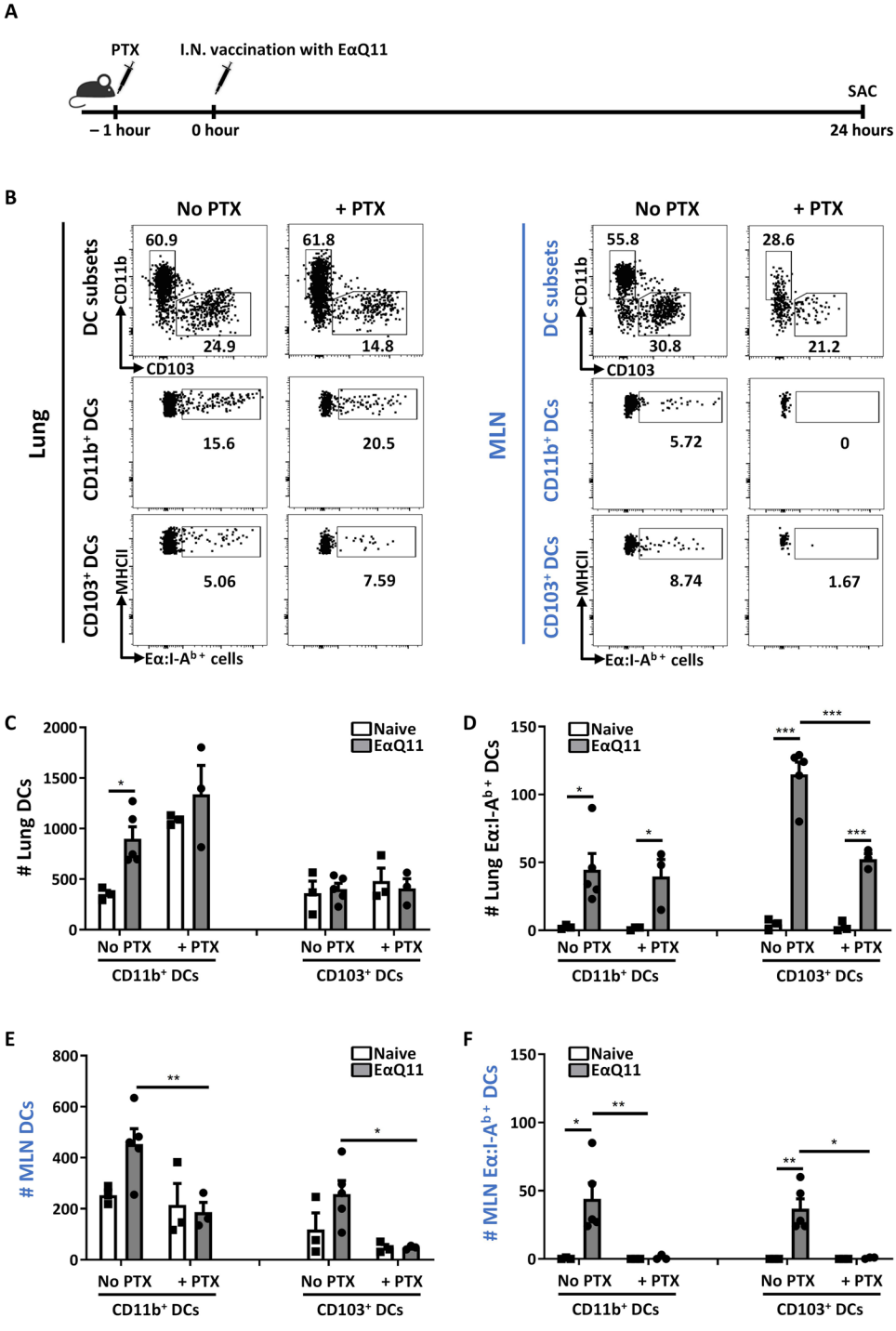

Fig. 4. Lung DCs are the major source of Eα:I-A^{b+} DCs in the MLNs after EαQ11 intranasal immunization. (**A**) Scheme of experiment. C57BL/6 mice were treated with PTX 1 hour before EαQ11 intranasal immunization to inhibit the migration of lung DCs into the MLNs. Lung and MLNs were collected at 24 hours after immunization, and Eα:I-A^{b+} cells were detected using the YAe mAb. (**B**) Representative flow cytometry plots displaying Eα presenting CD11b$^+$/CD103$^+$ DCs in lung (left; black labels) and MLN (right; blue labels), with or without PTX treatment. The number of total (**C**) and pEα:I-A^b–positive CD11b$^+$/CD103$^+$ (**D**) DCs in lung or total (**E**) and pEα:I-A^b–positive CD11b$^+$/CD103$^+$ (**F**) DCs in MLN. Each dot represents two pooled mice. Data shown are means ± SEM from three or more independent experiments. ***$P < 0.001$, **$P < 0.01$, and *$P < 0.05$ by unpaired, two-tailed t test (C to F).

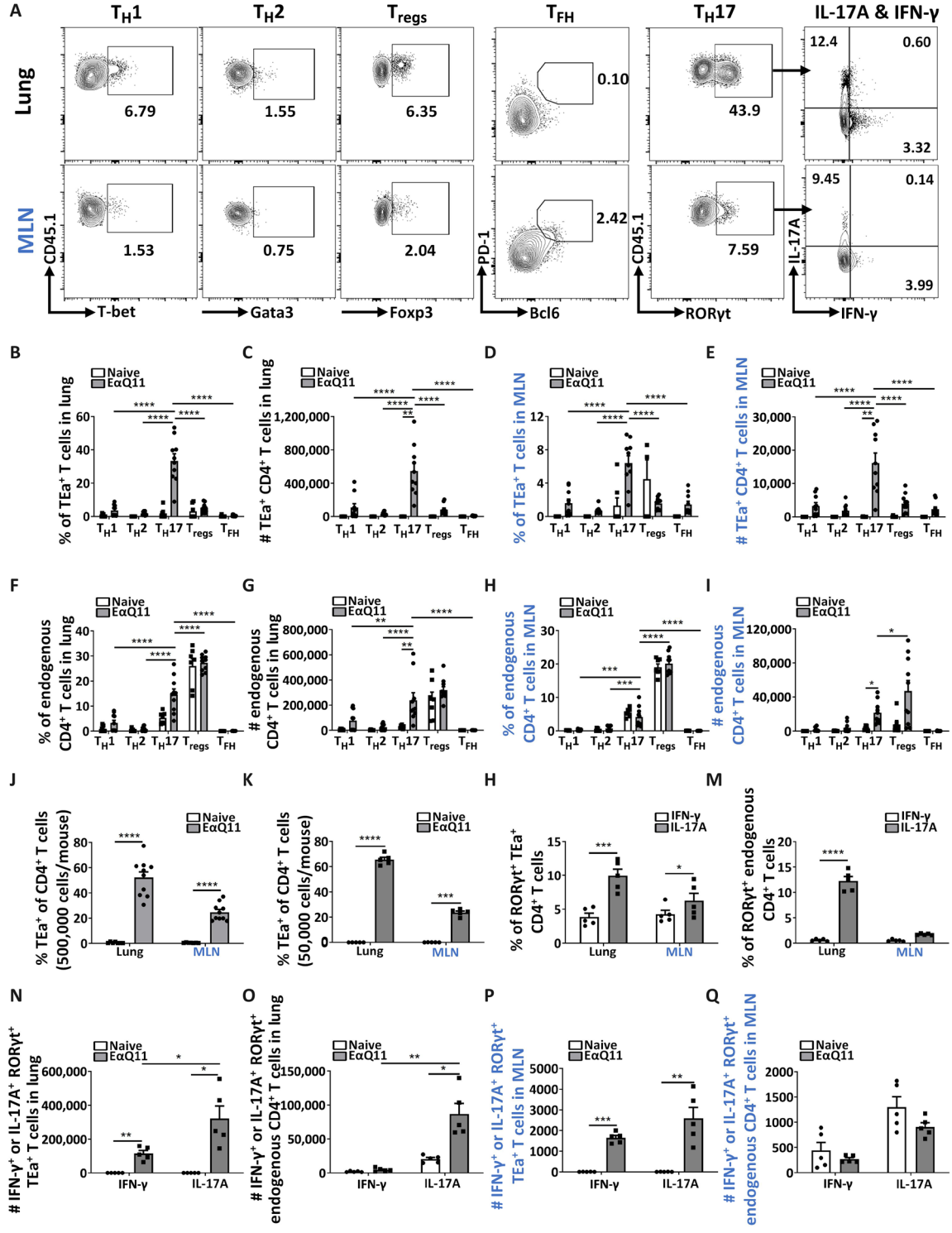

Fig. 5. T_H17 responses were elicited in lung and MLNs after EαQ11 intranasal immunization. To investigate antigen-specific effector subsets elicited after EαQ11 intranasal immunization, (**A** to **J**) 500,000 or (**K** to **Q**) 50,000 TEa T cells were AdT to each C57BL/6 mouse on 1 day before immunization and analyzed 5 or 6 days later. (A) Representative flow cytometry plots displaying TEa subsets: T_H1 (T-bet), T_H2 (Gata3), T_H17 (RORγt), T_{FH} (Bcl6 and PD-1), T_{regs} (Foxp3), IL-17A$^+$ RORγt$^+$, and IFN-γ$^+$ RORγt$^+$. Percentages of T_H1, T_H2, T_H17, T_{FH}, and T_{reg} TEa T cells in lung (B; black labels) and MLN (D; blue labels). Total numbers of T_H1, T_H2, T_H17, T_{FH}, and T_{reg} TEa T cells in lung (C) and MLN (E). (F and H) Percentages and (G and I) total numbers of T_H1, T_H2, T_H17, T_{FH}, and T_{reg} endogenous CD4$^+$ T cells in the (F and G) lung and (H and I) MLN. Percentage TEa T cells of CD4$^+$ T following (J) 500,000 (day 5 after immunization) or (K) 50,000 (day 6 after immunization) AdT TEa T cells. Percentage of (L) RORγt$^+$ of TEa or (M) endogenous CD4$^+$ T cells in the lung or MLN following EαQ11 immunization. Total numbers of IL-17A/IFN-γ–producing RORγt$^+$ (N and P) TEa and (O and Q) endogenous CD4$^+$ T cells in the (N and O) lung and (P and Q) MLN. Each dot represents one mouse. Data shown are means ± SEM from three or more independent experiments. ****$P < 0.0001$, **$P < 0.01$, and *$P < 0.05$ by one-way ANOVA (B to Q).

Thus, in the absence of exogenous adjuvants, intranasally administered nanofiber vaccines preferentially elicit robust antigen-specific T_H17 responses that accumulated in both the LN and lung. Last, we demonstrate that 500,000 and 50,000 AdT TEa cells per mouse responded similarly to intranasal EαQ11 immunization (Fig. 5, J and K). The RORγt$^+$ TEa (50,000 TEa per mouse) and endogenous T cells preferentially produced interleukin-17 (IL-17) over interferon-γ (IFN-γ), thus confirming their functionality (Fig. 5, L and M).

pEα:I-A^b–positive DCs stimulate TEa CD4$^+$ T cell proliferation in both the lung and draining LNs

To assess that immunization with EαQ11 nanofibers was able to stimulate T cell expansion, we AdT TEa CD4$^+$ T cells (500,000 per mouse) followed by EαQ11 intranasal vaccination (Fig. 6A). As anticipated, on day 5 after AdT, we observed significantly increased numbers of TEa T cells in the LN in EαQ11-immunized mice, compared to unimmunized mice (Fig. 6,B to D). We also observed significantly increased numbers of TEa T cells in the lung of EαQ11-immunized mice compared to unimmunized controls and noted that approximately 5- to 10-fold higher numbers of TEa cells were recovered from the lung compared to the draining LN.

Current paradigm is that DCs in secondary lymphoid organs stimulate T cell proliferation and differentiation into effector T cells that then migrate to sites of tissue inflammation. To test whether intranasal EαQ11 vaccination resulted in naïve T cell expansion in the LN and migration back to the lung, we treated vaccinated mice with FTY720 on the day of immunization (Fig. 6A). FTY720 is a sphingosine 1-phosphate (S1P) receptor agonist that inhibits lymphocyte egress from lymphoid tissues and their recirculation (*20*). Treatment with FTY720 blocked the egress of lymphocytes from secondary lymphoid organs into systemic circulation, thereby inducing lymphopenia in the blood (fig. S5A) and preventing the egress of naïve T cells primed in the LN. Despite the AdT of only naïve TEa cells (fig. S5B), we observed that treatment with FTY720 did not significantly decrease the number of TEa cells in the lung (Fig. 6, B and C). These unexpected observations raised the possibility that naïve TEa cells were primed in the MLN and also in the lung, the alternative possibility being that the high frequency of AdT TEa cells (500,000 per mouse) may have caused their spillover localization to the lung where they were primed locally. To control for the latter possibility, we repeated the experiment, but AdT only 10,000 TEa cells per mouse. We observed a reduction in the total number of TEa cells in the draining LNs of vaccinated mice treated with FTY720 compared to untreated but vaccinated controls, and a similar reduction in the lungs (fig. S5C). These observations are consistent with recent reports that FTY720 may directly inhibit distal TCR signaling events and T cell activation in an S1P receptor–independent manner (*21*, *22*). Together, these observations suggest that naïve TEa cells were being independently primed in the lungs and draining LNs, rather than being primed in the LN and then migrating to the lung.

To further test this possibility, we blocked naïve TEa T cell migration into the LN with anti–L-selectin mAb (MEL14), thereby inhibiting their priming in the LN (*23*). Mice treated with anti–L-selectin had significant 85% reduction in the numbers of TEa cells in the LN; in contrast, the total numbers of TEa cell accumulation in the lung were not significantly diminished (Fig. 6D). We also compared the expression of Ki-67 on the TEa cells, which marks recent exit from nonproliferative G_0 and G_1 phases and entry into the proliferative S, G_2, and M phases of cell cycle (*24*). Similar expression levels [measured by mean fluorescence intensity (MFI)] as well as percentage of Ki-67–expressing cells were observed in TEa cells in both the LN and lung (fig. S6, A to C). Collectively, these data are consistent with the conclusion that EαQ11 vaccination results in the independent priming of TEa cells in both the draining LN and lung.

To further confirm independent priming in the lung, we analyzed both AdT TEa T cell accumulation on day 3 versus day 5 after intranasal immunization. A significant increase in the percentage and total number of TEa cells was detected in the lung on day 3 after vaccination, whereas there was no significant increase in the MLN (Fig. 6, E and F). By day 5 after vaccination, there were significant increases in the percentage and number of TEa in the MLN and lung. These observations are congruent with the conclusion of independent priming by intranasal EαQ11 nanofibers of CD4$^+$ T cells in the lung.

We performed phenotyping of the TEa cells (fig. S8) and confirmed that on day 3 after immunization, the TEa cells in the lung had acquired central memory T cells (T_{CM}) (CD44$^+$CD62L$^+$) or effector memory T cells (T_{EM}) (CD44$^+$CD62L$^-$) phenotype at a 1:1 ratio, and were predominantly T_{EM} by day 5 (Fig. 6G). In contrast, TEa cells in the MLN remained at approximately a 1:1 ratio of T_{CM} and T_{EM} on day 5 after immunization (Fig. 6H). Last, we examined for markers of activation and tissue residence, namely, CD11a, CD69, and CD103 (figs. S7 and S8) (*25*). TEa cells in the lung and MLN up-regulated expression of CD11a by day 3, and CD103 by day 5 after EαQ11 immunization. An increase in the percentage of TEa cells expressing CD69 was detected by day 3 in the MLN and in the lung and LN by day 5 after vaccination. Collectively, these data demonstrating a detectable response by TEa cells to intranasal EαQ11 nanofibers in both the lung and LN as early as day 3 after immunization, but significantly increasing accumulation of TEa cells only in the lung, are consistent with independent T cell priming occurring in the lung and LNs.

DISCUSSION

Antigens that trigger immune responses can be soluble or present on physical scaffolds such as in virions, capsids, and cell membranes or attached to extracellular matrix. Immunologists have largely focused on soluble or membrane-associated molecules and the intracellular signals they trigger to elicit innate immune cell activation (*26*, *27*). In contrast, much less attention has been paid to testing whether the physical scaffold to which antigens are attached may also contribute to biological activity for DC activation and subsequent T cell responses. However, recent advances in tissue engineering and immune engineering suggest that the presentation of ligands in spatially organized patterns affects cell signaling (*28*). For instance, short sequences of DNA or RNA arranged around a nanoparticle core are more effective at activating a broad range of immune responses compared to free linear oligonucleotides (*29*). Adherent cells can respond to mechanical signals by altering their internal architecture through cytoskeletal networks that directly affect local signal transduction events and cell migratory behavior (*30*). More recently, Solis *et al.* (*4*) reported that myeloid cells in the lung are able to sense cyclical hydrostatic pressure to induce a proinflammatory gene expression that depends on PIEZO1. Last, our previous reports that antigens attached to Q11 nanofibers can elicit CD4, CD8, and antibody responses (*6*, *7*, *9*) in the absence of exogenous adjuvants or detectable local inflammation are consistent with the physical scaffold to which antigens are attached, contributing substantially to their immunogenicity.

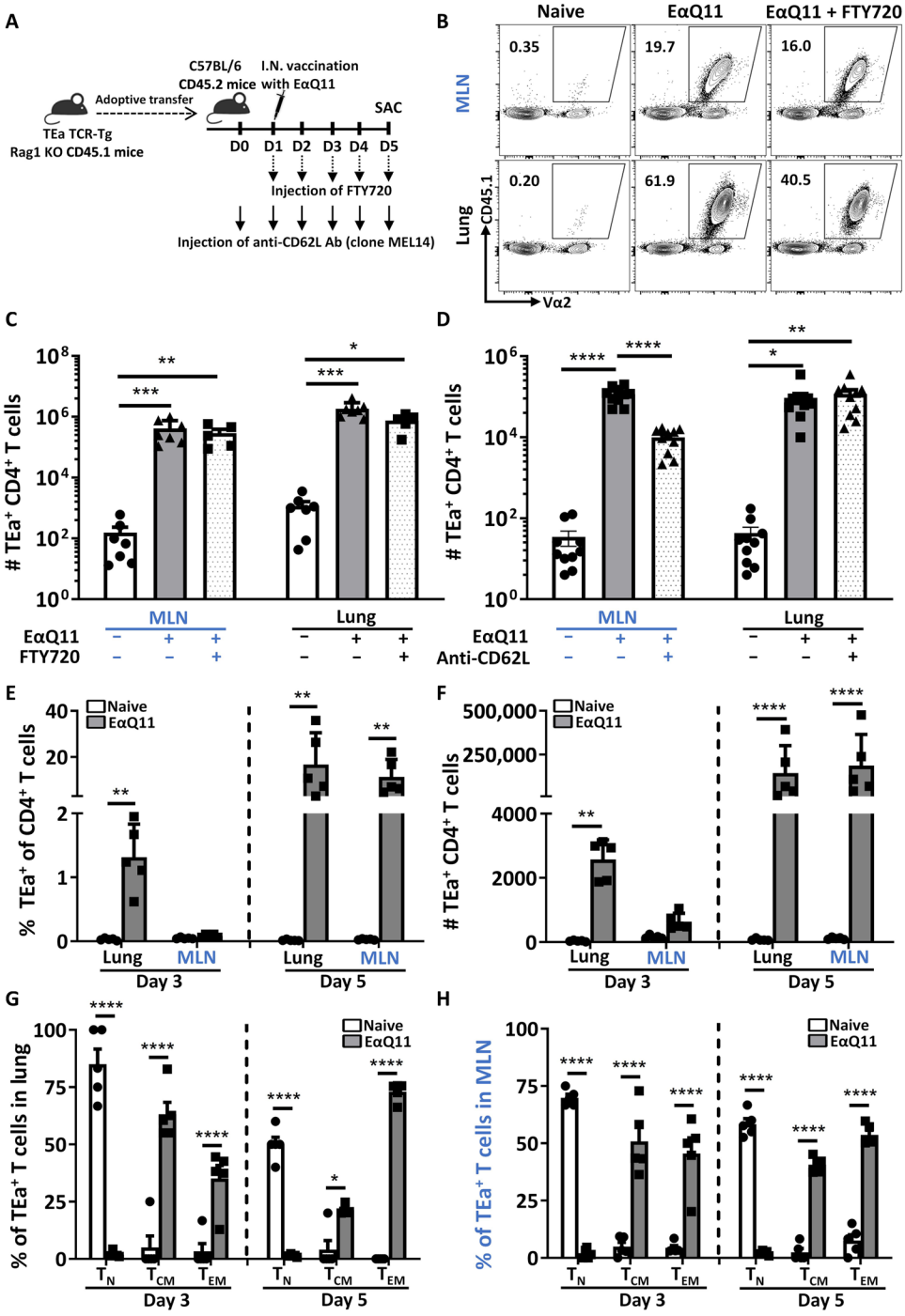

Fig. 6. TEa T cells proliferate in lung and MLNs after EαQ11 intranasal immunization. (**A**) Scheme of experiment. TEa T cells [500,000 (FTY720) or 50,000 (anti-CD62L blockade)] were adoptively transferred to each C57BL/6 mouse at 1 day before immunization. Five days later, single-cell suspensions were obtained from lung and MLNs, and donor TEa T cells were identified as $CD45.1^+V\alpha2^+$ gated on $CD4^+$ T cells. (**B**) Representative flow cytometry plots identifying TEa T cells in MLN (top; blue labels) and lung (bottom; black labels). (**C**) Total number of TEa T cells at 5 days after immunization with or without FTY720 treatment. (**D**) Total number of TEa T cells at 5 days after immunization, with or without anti-CD62L. (**E**) Percentage and (**F**) total number of TEa of $CD4^+$ T cells on days 3 and 5 after immunization (50,000 AdT TEa T cells). Percentages of T_N ($CD44^-CD62L^+$), T_{CM} ($CD44^+CD62L^+$), and T_{EM} ($CD44^+CD62L^-$) TEa T cells in lung (**G**) and MLN (**H**) on days 3 and 5 after immunization. Each dot represents one mouse. Data shown are means ± SEM from two or more independent experiments. $^{****}P < 0.0001$, $^{***}P < 0.001$, $^{**}P < 0.01$, and $^{*}P < 0.05$ by one-way ANOVA (C to H).

In this study, we provide data in support of this hypothesis, by showing that the intranasal delivery of a model antigen, pEα, attached to Q11 self-assembling nanofibers, results in pEα presentation by I-A^b on lung DCs, but not on lung $MHCII^{hi}$ B cells or macrophages. The induced expression of CD80 was higher on pEα:I-A^b–positive DCs compared to the pEα:I-A^b–negative DCs, suggesting that activation is optimally induced in the DCs presenting antigens derived from the Q11 nanofiber. We noticed that pEα:I-A^b–negative DCs in the lungs of intranasally vaccinated mice had modestly elevated CD80 expression, which could be due to bystander activation, or they are DCs that had taken up EαQ11 but were not presenting pEα:I-A^b at the time of analysis. Last, we found that intact nanofibers of 300 to 400 nm in length are necessary for successful presentation by lung DCs, whereas sheared EαQ11 (~100 nm) were not immunogenic. This finding is consistent with previous studies that also observed a loss in immunogenicity when Q11 nanofibers were disrupted by other means (*31*). Collectively, these data support our hypothesis that the physical scaffold contributes to the immunogenicity of intranasally delivered pEαQ1 nanofibers.

Lung $CD103^+$ DCs have been implicated in the cross-presentation of antigens to $CD8^+$ T cells, whereas $CD11b^+$ DCs preferentially stimulate $CD4^+$ T cell responses (*32*, *33*). We observed that EαQ11 intranasal vaccination triggered antigen presentation in both lung $CD103^+$ and $CD11b^+$ DCs and their migration to the draining LN. While there was a trend toward more total DCs in the LNs of vaccinated versus nonvaccinated mice, the fold increase in the number of pEα:I-A^b–expressing DCs was much higher and statistically significant. The kinetics of accumulation of pEα:I-A^b–expressing DCs in the draining LN is consistent with the migration of antigen-bearing lung DCs to the LN. Observations that PKH26-prelabeled DCs were the major subset of pEα:I-A^b–positive $DC11b^+$ and $CD103^+$ DC subsets in the draining LNs of pEαQ11 vaccinated mice, and the ability of PTX to inhibit DC accumulation, suggest that lung migratory DCs are the primary source of antigen-presenting DCs in the draining LN. Furthermore, pEα:I-A^b–positive DCs exhibited up-regulated CD80 expression, together with our published reports on the necessity of MyD88 (*6*, *9*), suggest that Q11 nanofibers trigger canonical activation preferentially in the subset of DCs presenting the EαQ11 vaccine antigens.

The current paradigm is that naïve T cells are primed in the draining LN, and the generated effector T cells exit the LN and migrate preferentially to the inflamed tissue harboring the vaccine antigen. We observed a significant accumulation of AdT naïve TEa cells in the draining LN of vaccinated mice compared to nonvaccinated controls on day 5 after vaccination. However, the percentage of TEa cells expressing the proliferation marker Ki-67 (fig. S6, A to C) was comparable in the lung and draining LN, and treatment with FTY720, which inhibits T cell egress from the LN, or anti-CD62L, which prevents naïve T cell entry into the LN, did not significantly reduce their numbers in the lung. Last, we show that on day 3 after immunization, significant increases in TEa cell numbers were detected in the lung but not in the MLN. Collectively, these observations challenge the prevailing paradigm of priming in the LN and egress of primed T cells into the lung and prompted the conclusion that priming with Q11 nanofibers elicits T cell responses independently in the draining LN as well as in the lung. Observations by Ciabattini *et al.* (*34*) that intranasal vaccination with recombinant bacteria triggered equivalent proliferation of AdT naïve $CD4^+$ OTII and $CD8^+$ OT1 T cells in the draining LN and lung on day 5 after intranasal immunization with OVA-expressing *Streptococcus gordonii* are consistent with this conclusion. Nevertheless, future investigations are required to test whether the ability of Q11 vaccines to prime in the lung generates long-term tissue-resident $CD4^+$ T cells. In addition, whether the ability to prime $CD4^+$ T cells in the lung is a feature restricted to intranasally delivered Q11 nanofibers and lung DCs or is applicable to other types or routes of vaccination and DCs from non-lung tissues remains to be clarified. It is tempting to speculate that lung DCs may be uniquely primed by cyclical hydrostatic pressure sensed in the lung, as has been described for lung myeloid cells (*4*), but not for DCs from other tissue sites. Last, it will be important to test whether T cells primed in the lungs or MLN skew preferentially toward T_H17, or whether each site differentially primes different $CD4^+$ effector subsets.

IL-17–producing cells play a critical role in immunity at mucosal surfaces, including the respiratory tract. During primary immune responses elicited by pathogens such as Gram-negative bacteria, IL-17 at the lung mucosal surface is produced by natural killer (NK) cells, γδ T cells, and group 3 innate lymphoid cells (ILCs) [reviewed in (*35*)]. However, after mucosal immunization, systemic and tissue-resident $\alpha\beta^+$ T_H17 cells predominate in immunity to Gram-positive bacteria, Gram-negative bacteria, and fungi (*36*–*38*). Currently, only a limited number of adjuvants can preferentially elicit T_H17 responses, and the use of nonspecifically proinflammatory adjuvants has raised concerns about inducing adverse effects following intranasal administration [reviewed in (*35*)]. Here, we demonstrate that EαQ11 intranasal vaccination elicited $CD4^+$ T cell responses, both in the LN and the lung, which were predominantly $ROR\gamma t^+$ T_H17 cells that preferentially secreted IL-17A. Collectively, these observations suggest that intranasal subunit vaccines formulated using the Q11 nanofiber platform may be effective for mucosal infections, where T_H17 responses are protective.

The predominant T_H17 response elicited by EαQ11 intranasal vaccination points to areas requiring further investigation. While T_H17 responses are protective for bacterial or fungal infections, they have been shown to be pathogenic for influenza infection and may exacerbate allergic airway inflammation susceptibility (*39*). Thus, future studies will focus on modifying the EαQ11 nanofiber to elicit T_H1, T_H2, T_{FH}, or T_{reg} responses. We previously reported that altering the CD4 epitope density on Q11 nanofiber skews T_H1/T_H2 to T_{FH} responses, suggesting that a similar approach may be able to modify T_H17 to T_H1 responses (*7*). Second, we have immunized naïve mice that were bred under specific pathogen–free facilities with minimal systemic and tissue-resident memory responses. It is possible that pretemplated immune responses within the lung, or even systematically, may alter the quality of the T cell responses elicited by nanofiber vaccines. Third, the specific intracellular signals that are triggered in lung DCs upon engagement Q11 scaffold and those that induce the processing of antigen and DC maturation have not been clarified and are areas of active investigation.

In summary, we show that EαQ11 intranasal vaccination, in the absence of exogenous adjuvants and minimal inflammation, results in the uptake and presentation of pEα on lung $CD103^+$ and $CD11b^+$ DCs, their up-regulation of CD80, and their migration to the draining LN. Peak numbers of pEα:I-A^b–expressing DCs in the lung were observed on days 1 to 3, and in the draining LN at days 3 to 5, after vaccination. T cell priming occurred in both the LN and lung and resulted in a predominantly T_H17 response, with minimal T_H1, T_H2,

T_{FH}, and T_{reg} responses. These observations suggest that Q11 nanofibers may be useful as a vaccine platform for bacterial and fungal infections in the respiratory tract, where safety of vaccination is critical and T_H17 cells are protective.

MATERIALS AND METHODS

Peptides and nanofiber preparation

Q11 (Ac-QQKFQFQFEQQ-$CONH_2$) and Eα_{52-68}Q11 (Ac-ASFEA-QGALANIAVDKA-SGSG-QQKFQFQFEQQ-$CONH_2$) were synthesized using standard Fmoc solid-phase chemistry, purified by high-performance liquid chromatography (HPLC) and matrix-assisted laser desorption/ionization mass spectrometry (MALDI-MS), and lypohilized as previously reported (*40*). To prepare the nanofibers, lyophilized peptides were weighed and intermixed as dry powders by vortexing for 30 min. Ultrapure water was added to form 8 mM total peptide solutions. After overnight incubation at 4°C, the peptide solution was diluted to 2 mM in 1× phosphate-buffered saline (PBS) by adding ultrapure water and sterile 10× PBS (catalog no. BP399-500, Fisher, Pittsburgh, PA, USA) and then incubated at room temperature for 3 hours. Sheared nanofibers were prepared by passing through a 0.2-μm membrane using the Avanti Mini Extruder (catalog no. 610000).

Electron microscopy

Peptide nanofibers were prepared at 2 mM as described for immunizations and diluted to 0.2 mM in 1× PBS. Then, 5 μl of diluted nanofiber solution was spotted onto Formvar/carbon-coated 400-mesh copper grids (Electron Microscopy Services, catalog no. FCF400-CU-SC). The sample was allowed to incubate for 1 min, washed five times with 0.2-μm filtered ultrapure water, and negatively stained for 1 min with 5 μl of 1% (w/v) uranyl acetate in water, followed by wicking of the staining solution with filter paper. Samples were imaged using an FEI Tecnai G^2 Twin TEM (FEI Company). For determination of nanofiber length from TEM images, nanofibers were manually traced using ImageJ software.

Mice and intranasal immunization

Six- to 8-week-old female C57BL/6 mice were purchased from Harlan-Envigo Laboratories. TEa TCR-Tg Rag1 knockout (KO) CD45.1 mice were a gift from M.-L. Alegre (The University of Chicago, Chicago, IL, USA). All mice were housed under specific pathogen–free conditions in the animal facilities at the University of Chicago. All procedures performed were approved by the Institutional Animal Care and Use Committees of the University of Chicago. For intranasal immunizations, mice were anesthetized, and 40 μl of vaccine formulations (2 mM total peptide) was slowly administered to one nostril using a micropipette.

In vivo labeling of lung DCs

Lung DCs were labeled in vivo by intranasal delivery of 40 μl of 1:100 diluted PKH26 dye (catalog no. MINI26-1KT, Sigma-Aldrich) at 4 hours before EaQ11 intranasal immunization.

PTX treatment

To inhibit lung DC migration, mice were treated with intranasal injection of 40 μl (0.04 μg) and intravenous injection of 200 μl (2 μg) of lyophilized PTX from Bordetella pertussis (catalog no. P7208-50UG, Sigma) or PBS alone as control.

Adoptive transfer of TEa T cells

Spleen and LNs were collected from TEa TCR-Tg CD45.1 mice [B6.Cg-Tg(Tcra,Tcrb)3Ayr/J, The Jackson Laboratory (JAX)], which were bred with CD45.1 C57BL/6 mice (B6.SJL-*Ptprc*^{a} *Pepc*^{b}/BoyJ, JAX). TEa T cells were isolated using a $CD4^+$ T Cell Isolation kit (Miltenyi Biotec, San Diego, CA, USA) according to the manufacturer's protocol. The purity of TEa T cells was confirmed to be >90% by flow cytometry. In some experiments, 500,000, 50,000 or 10,000 TEa T cells were injected into the tail vein of each recipient mouse 1 day before immunization. Five days later, single-cell suspensions were obtained from lung and MLNs for flow cytometry.

FTY720 treatment and L-selectin (anti-CD62L) blockade

Mice were treated with FTY720 (1 mg/kg; 20 μg per mouse) or PBS intraperitoneally daily starting on day 1 after immunization. To block access of circulating TEa T cells to LNs, mice were injected with 100 μg of anti-CD62L (clone MEL14, catalog no. 553147, BD Biosciences) or PBS as control intravenously daily 1 day before immunization.

Cell preparation and flow cytometry

Lungs and MLNs were collected at the indicated day after immunization. The tissues were mechanically disrupted and filtered through a 70-μm cell strainer to generate single-cell suspensions. Red blood cells (RBCs) were removed with ammonium-chloride-potassium (ACK) lysis buffer followed by washing with PBS twice. Cells were then counted and stained with the Zombie NIR Fixable Viability Kit (catalog no. 423105, BioLegend) and blocked with 2.4G2 antibody to exclude dead cells and to prevent unspecific binding. For cell surface staining, the following antibodies were used: anti-CD49b (DX5, catalog no. 563063, BD Biosciences), anti-TER119 (TER-119, catalog no. 563998, BD Biosciences), anti-CD19 (1D3, catalog no. 562701, BD Biosciences), anti-CD19 (1D3, catalog no.152405, BioLegend) anti-CD3 (145-2C11, catalog no. 100335, BioLegend), anti-CD45 (30-F11, catalog no. 103135, BioLegend), anti-CD64 (X54-5/7.1, catalog no. 139305, BioLegend), anti-CD24 (M1/69, catalog no. 101839, BioLegend), anti-CD103 (M290, catalog no. 565529, BD Biosciences), anti-CD11c (N418, catalog no. 117317, BioLegend), anti-CD11b (M1/70, catalog no. 101237, BioLegend), anti-Eα_{52-68} peptide bound to I-A^b (Y-Ae, catalog no. 11-5741-81, eBioscience), anti-MHCII (M5/114.15.2, catalog no. 107635, BioLegend), anti-CD80 (16-10A1, catalog no. 104737, BioLegend), anti-CD88 (20/70, catalog no. 743773, BD Biosciences), anti–Ly-6G (1A8-Ly6g, catalog no. 46-9668-80, eBioscience), anti–Siglec-F (E50-2440, catalog no. 740557, BD Biosciences), anti-MERTK (Mer, catalog no. 151505, BioLegend), anti-F4/80 (BM8, catalog no. 123127, BioLegend), anti-CD45.2 (104, catalog no. 109823, BioLegend), anti-CD45.1 (A20, catalog no. 110729, BioLegend), anti-CD4 (RM4-5, catalog no. 100528, BioLegend), anti-CD8 (53-6.7, catalog no. 100751, BioLegend), anti-CD44 (IM7, catalog no. 565480, BD Biosciences), anti-62L (MEL-14, catalog no. 104445, BioLegend), and anti-CXCR5 (L138D7, catalog no. 145513, BioLegend). For cell surface staining, cells were incubated with mAbs at 4°C for 30 min. For transcription factor staining, cells were fixed and permeabilized using the Foxp3/Transcription Factor Staining Buffer Set (catalog no. 00-5523, eBioscience) for 30 min at room temperature, followed by two washes with staining buffer (PBS + 2% fetal calf serum). Cells were then washed twice with Permeabilization Wash Buffer and incubated with anti-Foxp3 (FJK-16 s, catalog no. 11-5773-80, eBioscience), anti-RORγT (AFKJS-9, catalog no. 17-6988-80, eBioscience), and anti–T-bet (4B10, catalog no. 45-5825-80, eBioscience) overnight at 4°C. To detect IL-17A and IFN-γ

production, cells were cultured in the presence of phorbol 12-myristate 13-acetate (PMA) (50 ng/ml; catalog no. P1585-1MG, Sigma-Aldrich), ionomycin (750 ng/ml; catalog no. I3909-1ML, Sigma-Aldrich), and brefeldin A (5 μg/ml) (catalog no. B6542-5MG, Sigma-Aldrich) for 3 hours. After surface staining with the corresponding cocktail of antibodies, intracellular cytokine staining was sequentially performed with anti–IL-17A (TC11-18H10.1, catalog no. 506941, BioLegend) and anti–IFN-γ (XMG1.2, catalog no. 612769, BD Biosciences) using the same protocol as described above for transcription factor staining. Flow cytometry was performed on Cytek Aurora, BD LSRFortessa X-20, or BD LSRII and analyzed with FlowJo software (BD Biosciences).

Statistical analysis

Data are presented as means ± SEM. Statistical analyses were performed using GraphPad Prism software. Differences between groups were analyzed using one-way or two-way analysis of variance (ANOVA) with post hoc tests, or Student's *t* test where appropriate, as indicated in the figure legends.

SUPPLEMENTARY MATERIALS

Supplementary material for this article is available at http://advances.sciencemag.org/cgi/content/full/6/32/eaba0995/DC1

View/request a protocol for this paper from *Bio-protocol*.

REFERENCES AND NOTES

1. B. Bernocchi, R. Carpentier, D. Betbeder, Nasal nanovaccines. *Int. J. Pharm.* **530**, 128–138 (2017).
2. C. Y. Dombu, D. Betbeder, Airway delivery of peptides and proteins using nanoparticles. *Biomaterials* **34**, 516–525 (2013).
3. N. Petrovsky, Comparative safety of vaccine adjuvants: A summary of current evidence and future needs. *Drug Saf.* **38**, 1059–1074 (2015).
4. A. G. Solis, P. Bielecki, H. R. Steach, L. Sharma, C. C. D. Harman, S. Yun, M. R. de Zoete, J. N. Warnock, S. D. F. To, A. G. York, M. Mack, M. A. Schwartz, C. S. Dela Cruz, N. W. Palm, R. Jackson, R. A. Flavell, Mechanosensation of cyclical force by PIEZO1 is essential for innate immunity. *Nature* **573**, 69–74 (2019).
5. L. Zhao, A. Seth, N. Wibowo, C.-X. Zhao, N. Mitter, C. Yu, A. P. J. Middelberg, Nanoparticle vaccines. *Vaccine* **32**, 327–337 (2014).
6. J. Chen, R. R. Pompano, F. W. Santiago, L. Maillat, R. Sciammas, T. Sun, H. Han, D. J. Topham, A. S. Chong, J. H. Collier, The use of self-adjuvanting nanofiber vaccines to elicit high-affinity B cell responses to peptide antigens without inflammation. *Biomaterials* **34**, 8776–8785 (2013).
7. R. R. Pompano, J. Chen, E. A. Verbus, H. Han, A. Fridman, T. M. Neely, J. H. Collier, A. S. Chong, Titrating T-cell epitopes within self-assembled vaccines optimizes CD4+ helper T cell and antibody outputs. *Adv. Healthc. Mater.* **3**, 1898–1908 (2014).
8. J. S. Rudra, P. K. Tripathi, D. A. Hildeman, J. P. Jung, J. H. Collier, Immune responses to coiled coil supramolecular biomaterials. *Biomaterials* **31**, 8475–8483 (2010).
9. Y. Si, Y. Wen, S. H. Kelly, A. S. Chong, J. H. Collier, Intranasal delivery of adjuvant-free peptide nanofibers elicits resident $CD8^+$ T cell responses. *J. Control. Release* **282**, 120–130 (2018).
10. A. Rudensky, P. Preston-Hurlburt, S. C. Hong, A. Barlow, C. A. Janeway Jr., Sequence analysis of peptides bound to MHC class II molecules. *Nature* **353**, 622–627 (1991).
11. C. E. Grubin, S. Kovats, P. deRoos, A. Y. Rudensky, Deficient positive selection of CD4 T cells in mice displaying altered repertoires of MHC class II-bound self-peptides. *Immunity* **7**, 197–208 (1997).
12. M. Kopf, C. Schneider, S. P. Nobs, The development and function of lung-resident macrophages and dendritic cells. *Nat. Immunol.* **16**, 36–44 (2015).
13. Y. Si, Y. Wen, J. Chen, R. R. Pompano, H. Han, J. Collier, A. S. Chong, MyD88 in antigen-presenting cells is not required for $CD4^+$ T-cell responses during peptide nanofiber vaccination. *Medchemcomm* **9**, 138–148 (2018).
14. C. M. Freeman, J. L. Curtis, Lung dendritic cells: Shaping immune responses throughout chronic obstructive pulmonary disease progression. *Am. J. Respir. Cell Mol. Biol.* **56**, 152–159 (2017).
15. A. Hamilton-Easton, M. Eichelberger, Virus-specific antigen presentation by different subsets of cells from lung and mediastinal lymph node tissues of influenza virus-infected mice. *J. Virol.* **69**, 6359–6366 (1995).
16. P. Li, R. Zhang, H. Sun, L. Chen, F. Liu, C. Yao, M. Du, X. Jiang, PKH26 can transfer to host cells in vitro and vivo. *Stem Cells Dev.* **22**, 340–344 (2013).
17. H. E. Ghoneim, P. G. Thomas, J. A. McCullers, Depletion of alveolar macrophages during influenza infection facilitates bacterial superinfections. *J. Immunol.* **191**, 1250–1259 (2013).
18. R. Förster, A. Schubel, D. Breitfeld, E. Kremmer, I. Renner-Müller, E. Wolf, M. Lipp, CCR7 coordinates the primary immune response by establishing functional microenvironments in secondary lymphoid organs. *Cell* **99**, 23–33 (1999).
19. K. Sato, H. Kawasaki, H. Nagayama, M. Enomoto, C. Morimoto, K. Tadokoro, T. Juji, T. A. Takahashi, Signaling events following chemokine receptor ligation in human dendritic cells at different developmental stages. *Int. Immunol.* **13**, 167–179 (2001).
20. J. A. Cohen, J. Chun, Mechanisms of fingolimod's efficacy and adverse effects in multiple sclerosis. *Ann. Neurol.* **69**, 759–777 (2011).
21. A. Ntranos, O. Hall, D. P. Robinson, I. V. Grishkan, J. T. Schott, D. M. Tosi, S. L. Klein, P. A. Calabresi, A. R. Gocke, FTY720 impairs CD8 T-cell function independently of the sphingosine-1-phosphate pathway. *J. Neuroimmunol.* **270**, 13–21 (2014).
22. A. Baer, W. Colon-Moran, N. Bhattarai, Characterization of the effects of immunomodulatory drug fingolimod (FTY720) on human T cell receptor signaling pathways. *Sci. Rep.* **8**, 10910 (2018).
23. T. A. Yednock, E. C. Butcher, L. M. Stoolman, S. D. Rosen, Receptors involved in lymphocyte homing: Relationship between a carbohydrate-binding receptor and the MEL-14 antigen. *J. Cell Biol.* **104**, 725–731 (1987).
24. I. Miller, M. Min, C. Yang, C. Tian, S. Gookin, D. Carter, S. L. Spencer, Ki67 is a graded rather than a binary marker of proliferation versus quiescence. *Cell Rep.* **24**, 1105–1112.e5 (2018).
25. D. L. Turner, K. L. Bickham, J. J. Thome, C. Y. Kim, F. D'Ovidio, E. J. Wherry, D. L. Farber, Lung niches for the generation and maintenance of tissue-resident memory T cells. *Mucosal Immunol.* **7**, 501–510 (2014).
26. A. Iwasaki, R. Medzhitov, Regulation of adaptive immunity by the innate immune system. *Science* **327**, 291–295 (2010).
27. D. Schenten, S. A. Nish, S. Yu, X. Yan, H. K. Lee, I. Brodsky, L. Pasman, B. Yordy, F. T. Wunderlich, J. C. Brüning, H. Zhao, R. Medzhitov, Signaling through the adaptor molecule MyD88 in $CD4^+$ T cells is required to overcome suppression by regulatory T cells. *Immunity* **40**, 78–90 (2014).
28. S. H. Shabbir, M. M. Cleland, R. D. Goldman, M. Mrksich, Geometric control of vimentin intermediate filaments. *Biomaterials* **35**, 1359–1366 (2014).
29. G. Yamankurt, E. J. Berns, A. Xue, A. Lee, N. Bagheri, M. Mrksich, C. A. Mirkin, Exploration of the nanomedicine-design space with high-throughput screening and machine learning. *Nat. Biomed. Eng.* **3**, 318–327 (2019).
30. R. Sanghvi-Shah, G. F. Weber, Intermediate filaments at the junction of mechanotransduction, migration, and development. *Front. Cell Dev. Biol.* **5**, 81 (2017).
31. G. A. Hudalla, J. A. Modica, Y. F. Tian, J. S. Rudra, A. S. Chong, T. Sun, M. Mrksich, J. H. Collier, A self-adjuvanting supramolecular vaccine carrying a folded protein antigen. *Adv. Healthc. Mater.* **2**, 1114–1119 (2013).
32. J. K. Krishnaswamy, U. Gowthaman, B. Zhang, J. Mattsson, L. Szeponik, D. Liu, R. Wu, T. White, S. Calabro, L. Xu, M. A. Collet, M. Yurieva, S. Alsén, P. Fogelstrand, A. Walter, W. R. Heath, S. N. Mueller, U. Yrlid, A. Williams, S. C. Eisenbarth, Migratory $CD11b^+$ conventional dendritic cells induce T follicular helper cell-dependent antibody responses. *Sci. Immunol.* **2**, eaam9169 (2017).
33. A. N. Desch, G. J. Randolph, K. Murphy, E. L. Gautier, R. M. Kedl, M. H. Lahoud, I. Caminschi, K. Shortman, P. M. Henson, C. V. Jakubzick, $CD103^+$ pulmonary dendritic cells preferentially acquire and present apoptotic cell-associated antigen. *J. Exp. Med.* **208**, 1789–1797 (2011).
34. A. Ciabattini, E. Pettini, P. Andersen, G. Pozzi, D. Medaglini, Primary activation of antigen-specific naive $CD4^+$ and $CD8^+$ T cells following intranasal vaccination with recombinant bacteria. *Infect. Immun.* **76**, 5817–5825 (2008).
35. N. Iwanaga, J. K. Kolls, Updates on T helper type 17 immunity in respiratory disease. *Immunology* **156**, 3–8 (2019).
36. K. Chen, J. P. McAleer, Y. Lin, D. L. Paterson, M. Zheng, J. F. Alcorn, C. T. Weaver, J. K. Kolls, Th17 cells mediate clade-specific, serotype-independent mucosal immunity. *Immunity* **35**, 997–1009 (2011).
37. M. Wuthrich, T. T. Brandhorst, T. D. Sullivan, H. Filutowicz, A. Sterkel, D. Stewart, M. Li, T. Lerksuthirat, V. L. Bert, Z. T. Shen, G. Ostroff, G. S. Deepe Jr., C. Y. Hung, G. Cole, J. A. Walter, M. K. Jenkins, B. Klein, Calnexin induces expansion of antigen-specific $CD4^+$ T cells that confer immunity to fungal ascomycetes via conserved epitopes. *Cell Host Microbe* **17**, 452–465 (2015).
38. R. Gopal, L. Monin, S. Slight, U. Uche, E. Blanchard, B. A. F. Junecko, R. Ramos-Payan, C. L. Stallings, T. A. Reinhart, J. K. Kolls, D. Kaushal, U. Nagarajan, J. Rangel-Moreno, S. A. Khader, Unexpected role for IL-17 in protective immunity against hypervirulent *Mycobacterium tuberculosis* HN878 infection. *PLOS Pathog.* **10**, e1004099 (2014).
39. T.-Y. Shao, W. X. G. Ang, T. T. Jiang, F. S. Huang, H. Andersen, J. M. Kinder, G. Pham, A. R. Burg, B. Ruff, T. Gonzalez, G. K. K. Hershey, D. B. Haslam, S. S. Way, Commensal

Candida albicans positively calibrates systemic Th17 immunological responses. *Cell Host Microbe* **25**, 404–417.e6 (2019).
40. J. S. Rudra, Y. F. Tian, J. P. Jung, J. H. Collier, A self-assembling peptide acting as an immune adjuvant. *Proc. Natl. Acad. Sci. U.S.A.* **107**, 622–627 (2010).

Acknowledgments
Funding: This research was supported by the NIH (NIBIB 5R01EB009701; NIAID 5R01AI118182). S.H.K. is supported by the NSF Graduate Research Fellowship Program under grant no. DGE-1644868. A.I.S. received support from the NIH (R01 AI125644). D.F.C. received support from the NIH (F30HL137309 and T32GM007281). **Author contributions:** Y.S. performed most of the experiments, with assistance from F.Z., Q.T., and M.S.A., and generated the figures and performed statistical analyses of the data. L.S.S. performed the synthesis of EαQ11 peptides. S.H.K. provided information on the sheared EαQ11 peptides, and D.F.C. advised on lung DC recovery and flow analysis. A.I.S. assisted with the DC data interpretation. A.S.C. conceived the project, designed the experiments, and wrote the paper, in collaboration with J.H.C. All authors read and commented on the manuscript. **Competing interests:** J.H.C. is listed as an inventor on U.S. Patent No. 9,241,987, which is associated with the technology described. The patent covers the design and use of supramolecular peptide-polymer conjugates. J.H.C. is an inventor on a patent related to this work filed by USPTO (U.S. Patent 10,596,238, published on 24 March 2020). **Data and materials availability:** All data needed to evaluate the conclusions in the paper are present in the paper and/or the Supplementary Materials. Additional data related to this paper may be requested from the authors.

Submitted 4 November 2019
Accepted 25 June 2020
Published 7 August 2020
10.1126/sciadv.aba0995

Citation: Y. Si, Q. Tian, F. Zhao, S. H. Kelly, L. S. Shores, D. F. Camacho, A. I. Sperling, M. S. Andrade, J. H. Collier, A. S. Chong, Adjuvant-free nanofiber vaccine induces in situ lung dendritic cell activation and T_H17 responses. *Sci. Adv.* **6**, eaba0995 (2020).